IEEE Access
Multidisciplinary | Rapid Review | Open Access Journal

Received November 30, 2018, accepted December 22, 2018, date of publication January 1, 2019, date of current version January 23, 2019.

Digital Object Identifier 10.1109/ACCESS.2018.2890134

A Cruise Control Method for Connected Vehicle Systems Considering Side Vehicles Merging Behavior

TAO ZHANG, YUAN ZOU, (Senior Member, IEEE), XUDONG ZHANG, NINGYUAN GUO, AND WENWEI WANG

Beijing Collaborative and Innovative Center for Electric Vehicle, Beijing 100081, China
School of Mechanical Engineering, Beijing Institute of Technology, Beijing 100081, China

Corresponding author: Yuan Zou (zouyuanbit@163.com)

This work was supported in part by the National Key Research and Development Program of China under Grant 2017YFB0103801, in part by the National Natural Science Foundation of China under Grant 51775039 and Grant 51805030, and in part by the Beijing Institute of Technology Research Fund Program for Young Scholars.

ABSTRACT On the basis of wireless vehicle-to-vehicle communication, this paper proposes a superior control strategy for the merging behavior of connected cruise control (CCC) considering the effect of time delays. A novel range policy that integrates the consideration of side-vehicle merging scene is established, based on which a general strategy is proposed focusing on the acceleration control and incorporating various information delays. In this portion, the time-delay effect for the plant stability and head-to-tail string stability of CCC is explored and analyzed in detail. The results demonstrate that the traffic efficiency, the driving safety, and the ride comfort of CCC vehicles can be improved by the proposed method. In addition, the sensitivity study regarding the controller gain and the platoon's connectivity structure is exploited, which is proved to be of importance for system stability.

INDEX TERMS Connected cruise control (CCC), head-to-tail string, merging behavior, time delays.

I. INTRODUCTION

In recent years, thanks to the development of technologies such as automatic control, information communication, computer and artificial intelligence, intelligent and connected vehicles (ICV) have become the research hotspots in the field of transportation. By using wireless vehicle-to-vehicle (V2V) communication, driver or autopilot vehicle may obtain signal (including distance, velocity, and acceleration) about distant vehicles beyond the line of sight, which has great potential for enhancing safety of vehicles [1], [2]. And research has demonstrated their applicability to improve mobility [3], [4] and fuel economy [5].

A typical application of V2V communication is cooperative adaptive cruise control (CACC) [6], developed from the adaptive cruise control (ACC) technique [7], [8]. By grouping some vehicles equipped with V2V and ACC functions into a fixed platoon with the same velocity and headway, one may monitor the motion of a designated platoon leader. This fixed range policy and communication structure can improve the stability of the queue [9]. Variously experimental work in integrating CACC systems and wireless communication has been carried out in related researches and demonstration projects, such as PATH program in American, CHAUFFEUR project in Europe, SARTRE project, and Energy ITS [10]–[13]. Another demonstration of CACC is the Grand Cooperative Driving Challenge (GCDC), which has been held twice in 2011 and 2016 in the Netherlands. In GCDC, several vehicles cooperated in both urban and highway driving scenarios to facilitate the deployment and research of cooperative driving systems based on a combination of communication and state-of-the-art sensor fusion and control [14], [15]. Most research on CACC was focused on vehicle dynamics control in the longitudinal direction to achieve stable following and coordination of the platoon.

But in practical traffic scene, it is mostly not impossible for all vehicles equipped with expensive equipment or open communication units. Given this, the connected cruise control (CCC) is proposed, in which platoons can be formed based on the available communication and may be heterogeneous [16]–[18]. The host vehicle is actuated using acceleration information broadcast by other vehicles equipped

with V2V, and local headway and velocity information monitored by sensors. In fact, it is even unnecessary for other vehicles to broadcast their information to CCC vehicle. The item of non-CCC represents a human-drive vehicle with V2Vcommunication capability.

Lots of researches on platoon control have been developed recently, such as selection of spacing policies, influence of communication topology, and impact of dynamic heterogeneity [19]–[22]. Among them, the proportional-integral-differential (PID) controller is the most popular and favorite method for CACC and CCC, owing to its capacity of omitting vehicle dynamics (grade, air drag, and rolling resistance) and effectively restraining the tracking error. Other approaches are distributed controller design [15], [23], model predictive control [24], [25], and machine learning [26], [27] and so forth, mainly focusing on improving the driving safety and comfort.

The controller of the above solution can deal with a single longitudinal follow-up problem, however, and is unable to cope with the safety control under emergency side-vehicle combination scenario. For instance, vehicles in adjacent lanes suddenly merge into the platoon vehicle of the main lane, which is a common situation at highway ramp merges or lane closures. The phrase side-vehicle represents a vehicle with a merging trend in the adjacent lane. The National Highway Traffic Safety Administration (NHTSA) estimates that the lane changing and the merging collisions made up about 5% of all police-reported collisions in 2007 and accounted for about 0.5% of all fatal cases [28]. It is very important to design a CCC controller that can handle any side-vehicle merging interference behavior. Therefore, in addition to longitudinal control, it is also necessary to pay attention to the prediction of merging behavior.

Two common approaches are often used to establish the trajectory modeling problem, i.e., stochastic and kinematic. Stochastic models are able to establish a relationship between the behavior of the vehicle and the shape of lane change trajectory. The common stochastic modeling techniques are support vector machine [29], neural network [24], [30], Gaussian mixture model (GMM) [31], hidden Markov model [32], [33]. Although the stochastic model is always used to simulate and predict arbitrary nonlinear behavior, the accuracy of the results has a great relationship with the training samples. Besides, this type of method lacks exact physical meaning of the model parameters. In contrast, kinematic models describe lane-changing maneuvers in the form of physical meaning equations, and the trend of the lane change can be evaluated by the determined parameter value magnitude.

Reference [34] based on these real lane-change behavior data shows that the trajectory of the vehicle can be fitted with a fifth-order polynomial, which indicates that the lane-change process is a stable and smooth process without huge lateral fluctuation. However, these physical formulas cannot take into account the driver's behavioral characteristics, so when calculating some of the swaying merging parameters, the driver's intention to change lanes cannot be identified in time.

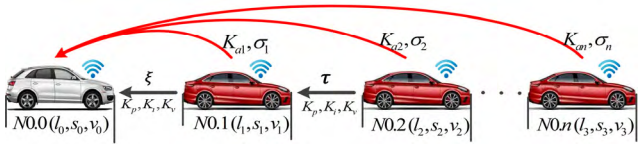

FIGURE 1. Connected vehicle systems network where a CCC vehicle (white) receives information from multiple non-CCC vehicles (red) ahead.

In this paper, we propose cruise control framework for CCC vehicles, considering the side vehicles merging behavior, the head-to-tail string stability and the delay time influences. Firstly, the merging data collected under practical driving situations is analyzed, by which the restively characteristic parameters can be selected. These parameters are converted into corresponding reference weights, a modified nonlinear range policy is introduced against the vehicles merging behavior case. And a new CCC-vehicle range policy is constructed that considering ahead vehicle and side-vehicle. Coordinated control range policy is necessary to harmonize flows and avoid collision for driver safety. A CCC controller with different type time delays, and consider integral term to eliminate the vehicle dynamics (air drag and rolling resistance) was be presented. With the corresponding design principles provided, we will prove the robustness of the proposed range policy and analyze the optimal gain parameters of the controller through stability analysis.

The remainders of this paper are organized as follows. A coordinated control range policy and a nonlinear CCC following model, are introduced in detail in Section 2. In Section 3, three scenes are employed to discuss, and we prove the head-to-tail string stability of the proposed strategy during merging process. The conclusion of this paper is in Section 4.

II. GUIDELINES FOR MANUSCRIPT PREPARATION

A heterogeneous vehicle network model is constructed with the consideration of the V2V interaction, the communication delay, the driver reaction time, as well as the human-drive merging behavior, as shown in Fig. 1.

The red arrow denotes the direction of information flow, l_n indexes the distance between vehicles, v_n means the drive velocity, and s_n indicates the vehicles' positions. Moreover, ξ is the sensing delay, and τ is the human reaction time. The other parameter symbols K_p, K_i, K_v, and K_a represent the gain coefficients of the controller, which will be introduced in Section 3. Note that σ_i denotes the communication delay between vehicles 0 and i, caused by intermittency and packet drops in V2V communication. Under this case, the CCC vehicle (namely the white car) is assumed to be capable of monitoring its preceding vehicles' position and velocity information, thereby performing the desired responses for drive comfort and safety. Reference [35] proposes that design

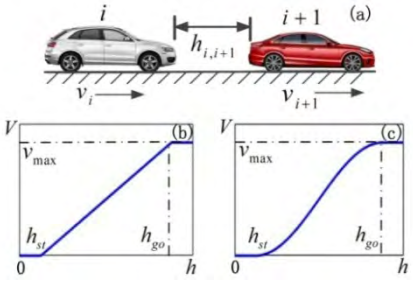

FIGURE 2. (a): Single-lane following of vehicle showing the headway and the velocity: (b): Range policy (2): (c): Range policy (3).

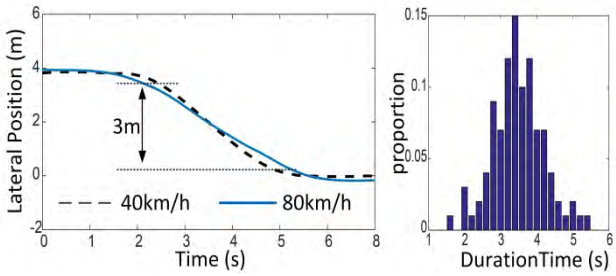

FIGURE 3. (a): Trajectories of two vehicle. (b): Probability distribution of lane-change duration times.

a link length estimator to identify the number of vehicles between a broadcast vehicle and a receiving vehicle. This article does not take this identification as a research focus. The motion of the vehicle immediately ahead can be monitored by human perception, range sensor, or V2V communication. In this paper, an assumption is imposed for the following study, that the CCC vehicles are equipped with range sensor and can monitor the immediately ahead vehicle in real time.

A. RANGE POLICY

The range policy is adopted to guide the CCC vehicle for holding a distance dependent velocity, where velocity range $v \in [0, v_{\max}]$ and distance range $h \in [0, \infty]$. For human drivers [36], the range policy can be presented as:

$$V(h) = \begin{cases} 0 & if\ h \le h_{st}, \\ F(h) & if\ h_{st} < h < h_{go}, \\ v_{\max} & if\ h \ge h_{go}, \end{cases} \quad (1)$$

where $V(h)$ indicates the desired velocity related to the headway h. $h_{i,i+1}$ represents the distance between the vehicle i and $i+1$. Two distance thresholds h_{st} and h_{go} are adopted here for arranging the desired velocity, respectively, whose corresponding objective velocity is 0 and $v_{\max}$, respectively. More intuitive illustration can be found in Fig. 2(b). When the headway is lower or greater than a certain distance, $V(h)$ is limited so that the appropriate safe vehicle gap can be guaranteed. Between the two distance thresholds, a monotonously increasing relationship $F(h)$ is imposed for the sake of smoothly tracking control.

Range policy with the linear function (2) [14], which corresponds to the constant time headway $t_h = (h_{go} - h_{st})/v_{\max}$, is shown in Fig. 2(b). Since the gradient discontinuity of $V(h)$ will causes the jerk discontinuity (especially when $h = h_{st}$ and $h = h_{go}$) and further lead to the undesirable drive comfort, a nonlinear relationship (3) including cosine function is applied for smoothing:

$$F(h) = v_{\max} \frac{h - h_{st}}{h_{go} - h_{st}}, \quad (2)$$

$$F(h) = \frac{v_{\max}}{2} \left(1 - \cos(\pi \frac{h - h_{st}}{h_{go} - h_{st}})\right), \quad (3)$$

In this paper, all human-drive vehicles are assumed to adopt the range policy function of (3), and all vehicles are trying to maintain the uniform traffic flow equilibrium:

$$h^* \equiv h_{i,i+1}(t) \equiv s_{i+1} - s_i - l_{i+1}, \quad v^* \equiv v_i(t) \equiv V(h^*), \quad (4)$$

for $i = 0, \ldots, n$, and the headway $h_{i,i+1}$ contains the distance from the immediately ahead vehicle.

Faster vehicle speed means that the relative distance between the vehicles is larger, and the larger gap is more likely to induce the driver of the side lane to change lanes. One hundred groups of side-vehicle lane change parameters are collected from the actual road environment, including vehicle speed, steering wheel angle, acceleration, and relative distance from the host CCC-vehicle, are employed to determine which one is the most characteristic. The statistical results show that most of the vehicle lateral acceleration is relatively small, which is not conducive to establish the relationship with the merging behavior. Wheel angle and lateral speed have the same changing trend, and there is no absolute correlation between longitudinal position and speed during the lane change. In addition, during the middle period for the whole lane change process, the lateral movement speed is nearly constant, which can be explained by Fig 3(a). The middle displacement of its lateral movement track is approximately close to a straight line.

Reference [34] illustrates that the lane changing time satisfies the normal distribution, and more than 99.7% vehicles complete a lane change within 12s. In this paper, only the middle region of the lane change trajectory is focused. Fig. 3(b) statistics the lane change duration within 3m of the transverse displacement span, and more than 90% duration times is longer than 2.8s. In China, the standard lane width of four-lanes, six lanes, and eight lanes under expressway, is 2*7.5m, 2*11.25m, and 2*15m. Considering the duration time and lane widths, most lateral movement speed of the vehicle may be less than 1m/s during the lane changing process.

The wide of most cars are less than 1.8m, and which means the average transverse distance of vehicles in two lanes is less than 1.95m. In a single lane, there are activity areas of nearly 1m on each side of the vehicle. In order to obtain a predicted time close to 1s, the unilateral monitoring area is determined within the range of 1m in this paper. To clarify both the lateral motion of the vehicle and the trend of its motion, we select the most characteristic lateral relative distance and lateral

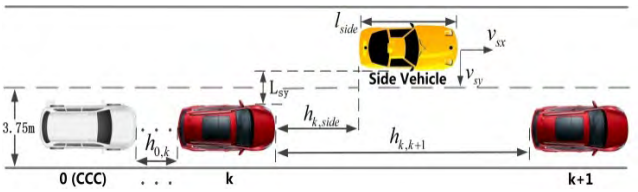

FIGURE 4. The scenario when the vehicle merging into target platoon.

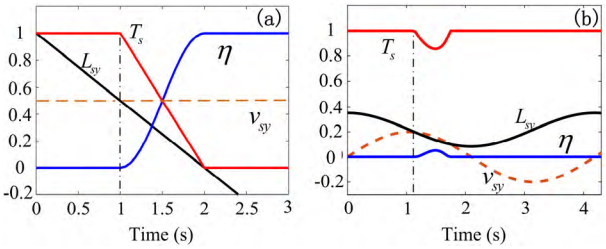

FIGURE 5. Parameter changes during the merging process.

relative velocity to establish a function of time. Then, a novel CCC vehicle range policy can be proposed:

$$T_s = \begin{cases} 1 & if\ L_{sy} > 1\ or\ (L_{sy}/v_{sy}) > 1\ or\ v_{sy} \le 0, \\ L_{sy}/v_{sy} & if\ 1 \ge L_{sy} > 0 \quad and\ v_{sy} > 0, \\ 0 & L_{sy} \le 0, \end{cases} \tag{5}$$

$$\eta = 0.5 + 0.5\cos(\pi T_s), \tag{6}$$

$$h_{(0,1)}(t) = \frac{\eta h_{k,side}(t) + (1-\eta)h_{k,k+1}(t) + h_{0,k}(t)}{k+1}, \tag{7}$$

$$F(h) = \frac{v_{\max}}{2}\left(1 - \cos(\pi \frac{h_{(0,1)} - h_{st}}{h_{go} - h_{st}})\right), \tag{8}$$

where $k = 0, \ldots, n$. The new distance function (7) can consider the distance from the immediately ahead vehicle, and the distance from the side-vehicle and other non-CCC vehicles in front, simultaneously. When there is no side vehicles nearby, it means that $h_{(0,1)} = h_{0,1}$ and $\eta = 0$.

As shown in Fig. 4, yellow side-vehicle represents the human-drive vehicle who intends to merge into vehicle k and $k+1$, and maintains the same constant longitudinal speed as preceding vehicles $k+1$ in the target lane. Under normal circumstances, the effective distance range $h_{k,side} \in (l_{side}, h_{k,k+1} - l_{side})$, and extreme distance conditions do not occur. Here $h_{k,side}$ denotes the distance between vehicle k and side-vehicle, v_{sy} is the lateral speed of the side-vehicle, and the lateral distance is denoted by L_{sy}, which can be calculated by vehicle coordinate position base on the inertial navigation system. $h_{0,k}$ is used to denote the distance between vehicle 0 and k, and $h_{k,k+1}$ represents the distance of vehicle k and vehicle $k+1$. The parameter η in the CCC range policy (8) indicates the coefficient of side-vehicle distance, which will be described in detail below.

The transverse velocity fluctuation in the middle course of lane change is small and can be considered as a fixed value. $T_s = L_{sy}/v_{sy}$ is arranged to remain merging time before side-vehicle merging into target lane when overlap in the longitudinal direction with the queue vehicle. The transverse velocity less than 1m/s and the monitoring area as far as 1m ensured the prediction time up to 1s. To promote the recognition effectiveness of merging behavior, some constraints are imposed:

1) With normalization constraints, the maximum value of T_s is limited to 1s. Additionally, when $L_{sy} > 1$m, or $T_s > 1$m, T_s is set to 1s. This means that if a side-vehicle merges into the target lane at a lateral velocity $v_{sy} = 0.5$m/s within the lateral distance of 1m, T_s is set less than 1s only when the horizontal distance decreases to 0.5m.

2) When $v_{sy} \le 0$m/s, i.e., the side-vehicle is moving far away from the target lane, T_s sets to 1s. When vehicles reach to a lateral position $L_{sy} \le 0$m, the vehicle merging behavior is considered to be happened definitely and T_s is set zero.

In (5), T_s is a time coefficient indicating that the edge of side-vehicle reaches to the overlap, and (6) is applied to invert and smooth the time function (5). In this situation, instantaneous remain merging time is mapping to a factor of $\eta \in [0, 1] \in [0, 1]$, and $\eta = 0$ indicates that this is no merging behavior occurred, and $\eta = 1$ indicates that the merging process has been completed. In practice, there may be some vehicles that are quite close to the host vehicle, and they do not intend to change lanes. But no matter how close the distance is, as long as there is no relative velocity, the calculation of T_s is set 0, that is, no merging behavior occurs. In the actual monitoring data collection, the data with the transverse velocity less than 0.1 is filtered out, and the mean value method is adopted to reduce the acquisition noise of the sensor.

Now two driving conditions are considered to illustrate more intuitively, as shown in Fig.5. One represents that the side-vehicle is approaching the target line with a fixed lateral speed $v_{sy} = 0.5$m/s at the distance of $L_{sy} = 1$m, as shown in Fig. 5(a). The other is that the side-vehicle fluctuates left and right laterally with a sinusoidal lateral speed $v_{sy} = 0.2\sin(3\pi)$m/s v $= 0.2\sin(3\pi)$ at the distance of $L_{sy} = 0.35$m, which never entered the target lane as the black lines shown in Fig.5 (b).

In scene (a), merging coefficient η smoothly increases as the T_s linearly reduced. The coefficient T_s starts to change only when $L_{sy} < 0.5$m. In scene (b), the low-speed lateral sway in the near-distance, produce a small weight coefficient of η. Meanwhile, the amplitude change of η is smaller than T_s, which means that the effect of lateral speed fluctuations can be buffered through the designed new range policy. Here, assume the CCC vehicle can identify the number of vehicles, even though the CCC vehicle is not receiving messages from the ith vehicle ahead. On the other hand, upper recognition system can automatically update the numbers when side-vehicle has completed the merging behavior by using other V2V information. In general, such identification is a challenging problem and is not our scope in this paper.

B. NONLINEAR CONTROL DESIGN

With the complex nonlinear features of vehicle dynamic, the integral term z_0 should be included in controller to eliminate disturbance like air-drag and the rolling resistance, which can make the system steady-state error converge to zero. Considering the single-lane configuration as shown in Fig. 1, a nonlinear CCC controller is adopted regulate the acceleration:

$$\begin{aligned}\dot{v}_0(t) &= K_p{}^*\dot{z}_0(t-\xi) + K_i{}^* z_0(t-\xi) \\ &\quad + K_v{}^*\dot{h}_{(0,1)}(t-\xi) + K_{ai}{}^*\sum_{i=1}^{n}\gamma_i{}^*\dot{v}_i(\mathrm{t}-\sigma_i), \\ \dot{z}_0(t) &= V(h_{(0,1)}(t)) - v_0(t), \\ \dot{h}_{(0,1)}(t) &= v_1(t) - v_0(t),\end{aligned} \tag{9}$$

where $i = 1, \ldots,$n, and $\gamma_i = 1$. Here the dot stands for differentiation with respect to time t. K_* indicates the related gain coefficient for the error items in (9). In particular, the gain γ_i is set to zero when the messages from the ith vehicle ahead missing or not present. Note that K_p and K_v have the unit 1/s, and K_i have the unit $1/s^2$. Indeed, K_a is a dimensionless quantity.

It should be noted that, only the acceleration of the preceding vehicles is considered in the proposed controller, and that said, the position and speed information of the remote vehicle cannot be applied, as the acceleration information can reflect the movement trend of the vehicle. In practice, for preceding vehicles, the respective distance gaps and the speed are always inconsistent. If the controller introduces the position information of the remote vehicle, a large amount of error data will be introduced in the actual application, which will affect the control effect.

Characterizing the system dynamics with a large number of independent parameters is typically not feasible. In order to make the analysis tractable, we assume the gain factor for acceleration errors is same, namely $K_a = K_{an}$. In practice, there are three kinds of delay: human reaction time τ, sensing delay ξ, and communication delay σ. Generally, the human reaction time $\tau \approx 0.4 - 1.5[s]$ and sensing delay $\xi \approx 0.1 - 0.2[s]$. Communication delays are time-varying stochastically [37], and arise from intermittency and packet drops [38], which are commonly deemed as $\sigma \approx 0.1 - 0.4[s]$.

Similarly, the driving behavior of the preceding non-CCC vehicles is described by the car-following model,

$$\begin{aligned}\dot{v}_i(t) &= K_p{}^*\dot{z}_i(t-\tau) + K_i{}^* z_i(t-\tau) + K_v{}^*\dot{h}_i(t-\tau), \\ \dot{z}_i(t) &= V(h_i(t)) - v_i(t), \\ \dot{h}_i(t) &= v_{i+1}(t) - v_i(t),\end{aligned} \tag{10}$$

where $i = 1, \ldots,$n. For simplicity, all drivers are considered as identical and all the non-CCC vehicles use the same car-following model.

Based on the controller and range policy, the CCC vehicle intends to keep a velocity dependent distance from the vehicle ahead. Thus, when the vehicles ahead travel with a constant velocity v^* and a constant headway h^* simultaneously, the CCC vehicle can reach its desired equilibrium $v^* = V(h^*)$v* = V(h*). Similarly, there also exists an equilibrium z^*, and the perturbations can be defined as:

$$\tilde{v}_i(t) = v_i(t) - v^*, \quad \tilde{h}_i(t) = h_i(t) - h^*, \ \tilde{z}_i(t) = z_i(t) - z^*, \tag{11}$$

for $i = 0, \ldots,$n, and linearize (9, 10), this yields:

$$\begin{aligned}\dot{\tilde{v}}_0(t) &= K_p * \dot{\tilde{z}}_0(t-\xi) + K_i * \tilde{z}_0(t-\xi) \\ &\quad + K_v * \dot{\tilde{h}}_{(0,1)}(t-\zeta) + K_a * \sum_{i=1}^{n}\gamma_i * \dot{\tilde{v}}_i(\mathrm{t}-\sigma), \\ \dot{\tilde{z}}_0(t) &= f^*\tilde{h}_{(0,1)}(t) - \tilde{v}_0(t), \\ \dot{\tilde{h}}_{(0,1)}(t) &= \tilde{v}_1(t) - \tilde{v}_0(t),\end{aligned} \tag{12}$$

for the CCC vehicle, and

$$\begin{aligned}\dot{\tilde{v}}_i(t) &= K_p{}^*\dot{\tilde{z}}_i(t-\tau) + K_i{}^*\tilde{z}_i(t-\tau) + K_v * \dot{\tilde{h}}_i(t-\tau), \\ \dot{\tilde{z}}_i(t) &= f^*\tilde{h}_{i,i+1}(t) - \tilde{v}_i(t), \\ \dot{\tilde{h}}_{i,i+1}(t) &= \tilde{v}_{i+1}(t) - \tilde{v}_i(t),\end{aligned} \tag{13}$$

for the non-CCC vehicle, $i = 1, \ldots, n$. Here $f^* = V(h^*)$ is the derivative of the range policy (1) at the equilibrium of $h = h^*$, and the corresponding time headway is $t_h = 1/f^*$. In practice, the equilibrium status is determined by the velocity of the head vehicle, and a larger value of f^* produces more aggressive car-following behaviors, which makes it more difficult to maintain uniform traffic flow. String stability is achieved when velocity fluctuations are attenuated as they propagate upstream [39]. The scenario with the worst stability, i.e., $h^* = 20$m and $v^* = V(h^*) = 15$ m/s, is presented as an example for description and analysis. Under this scenario, the largest derivative $f^* = \pi/2\ [1/s]$ and the smallest equilibrium time headway $t_h \approx 0.6$ s are obtained. Based on the highway traffic data [36], $v_{\max} = 30$ m/s, $h_{st} = 5$ m and $h_{go} = 35$m are used in this paper.

Build a head-to-tail transfer function, and consider $\tilde{v}_n$ as the input and $\tilde{v}_0$ as the output. After Laplace transform of system (12) and (13) under zero initial condition, the head-to-tail transfer function can be obtained:

$$\Gamma_{i,i+1}(s) = \frac{\tilde{V}_i(s)}{\tilde{V}_{i+1}(s)} = \frac{F(s)}{G(s)}, \tag{14}$$

for the non-CCC vehicle ($i = 1, \ldots$ n), and

$$\begin{aligned}\Gamma_{0,i}(s) &= \frac{\tilde{V}_0(s)}{\tilde{V}_n(s)} \\ &= \left(\frac{F(s)}{G(s)}\right)^i \left(\frac{G(s)}{H(s)}\right)\left(1 + \sum_{k=1}^{i}\frac{E_k(s)(G(s))^{k-1}}{(F(s))^k}\right),\end{aligned} \tag{15}$$

for the CCC vehicle ($i = 1, \ldots n, i > k$). $\tilde{V}_i(s)$ denotes the Laplace transform of $\tilde{v}_i(s)$, and

$$\begin{aligned} F(s) &= K_v s^2 + f^* K_p s + f^* K_i, \\ E_k(s) &= K_{ak}\gamma_k s^3 e^{(\xi-\sigma)s}, \\ H(s) &= s^3 e^{\xi s} + (K_p + K_v)s^2 + (f^* K_p + K_i)s + f^* K_i, \\ G(s) &= s^3 e^{\tau s} + (K_p + K_v)s^2 + (f^* K_p + K_i)s + f^* K_i \end{aligned} \quad (16)$$

In the following, the control system stability, including the plant stability and the string stability, will be illustrated with comprehensive analysis.

III. LINEAR STABILITY ANALYSIS AND STABILITY CHARTS

In this section, plant stability and head-to-tail string stability of CCC vehicle are analyzed according to the head-to-tail transfer function (14). In particular, the domains of stability charts in the different parameter space (K_p, K_i, K_v, K_a, σ, and ξ) are described. Plant stability means that the leader is driving with constant speed and the CCC vehicle can reach this speed. String stability means that the speed fluctuations of leader vehicle can be attenuated during transfer backward [20], [22].

To realize plant stability, the poles of the controller (15) have to be located in the left-half complex plane. That said, by substituting $\pm j\Omega$ ($j^2 = -1, \Omega \geq 0$) into the characteristic equation $D_i(s) = (G(s))^{i-1}H(s)$, it should satisfy $D(\pm j\Omega) = 0$, namely:

$$\mathrm{Re}(D(j\Omega)) = 0, \quad \mathrm{Im}(D(j\Omega)) = 0. \quad (17)$$

It can be observed that the characteristic equation $D_i(s)$ does not contain the coefficient of K_a. This is because the acceleration feedback has no relationship with the plant stability in this simple model. From (17), the plant stability boundaries related to control parameters can be gained and illustrated in the (K_p, K_v)-plane.

In the following, the string stability analysis is performed according to the head-to-tail transfer function. A disturbance with frequency ω from the head vehicle will be amplified by the ratio of $\left|\Gamma_{0,i}(j\omega)\right|$, when disturbance reaches the tail vehicle. Thus, the necessary and sufficient condition for head-to-tail string stability are given by

$$\left|\Gamma_{0,i}(j\omega)\right| < 1, \quad \forall\omega > 0. \quad (18)$$

For head-to-tail string stability boundary, $\left|\Gamma_{0,i}(j\omega)\right| = 1$ and the stability boundary is given by the equations :

$$\left|\Gamma_{0,i}(j\omega_{cr})\right| = 1, \left|\Gamma_{0,i}(j\omega_{cr})\right|' = 0, \left|\Gamma_{0,i}(j\omega_{cr})\right|'' < 0, \quad (19)$$

where ω_{cr} is the critical frequency that the maximum occurs. Note that $\left|\Gamma_{0,i}(j\omega)\right| < 1$ also depends on the system parameters K_p, K_i, K_v, K_a, σ, ξ, and τ. Here the control coefficients are imposed to be same with previous. By solving (19), the head-to-tail string stability boundaries are gained. Since it is impossible to solve it analytically, the continuation package DDE-BIFTOOL [40] of MATLAB is employed to obtain numerical solutions with differently critical frequency ω_{cr}.

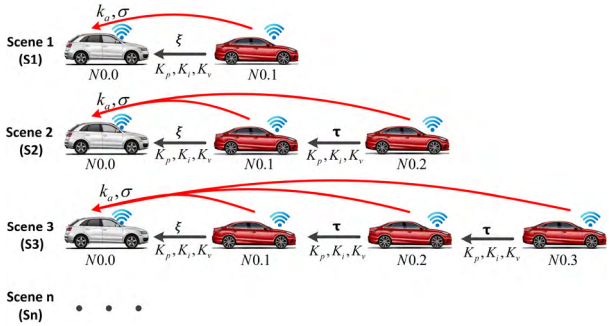

FIGURE 6. Network with different numbers of vehicles.

A. STABILITY DIAGRAMS FOR S_1

In this portion, the stability for plant and string are discussed in depth under the cases of monitoring different numbers of vehicles ahead. For discussion, the schematic diagram of different communication topologies is shown in Fig.6. In the scene 1 (S_1), the CCC vehicle receives acceleration signals from the vehicle immediately ahead only, and the corresponding characteristic equation is,

$$D_1(S) = H(s) = s^3 e^{\xi s} + (K_p + K_v)s^2 + (fK_p + K_i)s + fK_i = 0. \quad (20)$$

Solving (20) with fixed value K_i, the plant stability boundary can be presented in parametric form:

$$\begin{aligned} K_p &= (\Omega^2 \cos(\Omega\xi) - K_i)/f^*, \\ K_v &= (\Omega^3 \sin(\Omega\xi) + f^* K_i)/\left(\Omega^2\right) - K_p. \end{aligned} \quad (21)$$

Fig.7 (a) shows the corresponding plant stability boundary regarding (21), where the red solid curve, composed of the light and dark grey areas, for $K_i = 0.5$ and $\xi = 0.2$s. It has been proved that plant stability is guaranteed if the zeros and poles are restricted in this enveloping area [41]. Simultaneously, the corresponding critical frequency Ω (red curve) increases along the boundary with $K_v = 0.5$, as shown in Fig. 7(b). The low and high frequency oscillations correspond to the lower and upper part of the plant stability boundary respectively. Points A to C are marked to show how the plant stability changes when crossing the plant stability boundary, and the leading eigenvalues in the complex plane are plotted in Fig. 7(e)-7(g), respectively. A pair of complex conjugate roots crosses the imaginary axis at $\pm i$, when moving from point A to point C.

From (14), the head-to-tail transfer function of S_1 can be furnished,

$$\Gamma_{0,1}(s) = \frac{\tilde{V}_0(s)}{\tilde{V}_1(s)} = \frac{F(s) + E_1(s)}{H(s)} \quad (22)$$

Without considering the acceleration term, the head-to-tail transfer function of S_1 is shown as:

$$\Gamma_{0,1}(s) = \frac{\tilde{V}_0(s)}{\tilde{V}_1(s)} = \frac{F(s)}{H(s)}, \quad (23)$$

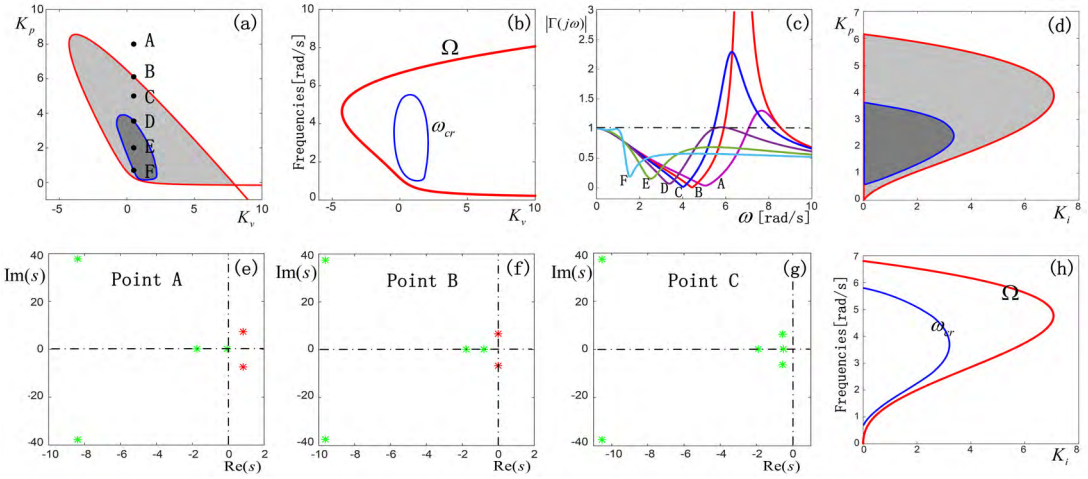

FIGURE 7. (a): Stability diagram of S_1 in the (K_p, K_v)-plane; (b): Critical stable frequency curve of Fig. 7(a); (c): Bode plots corresponding to cases A–F. (d): Stability diagram of S_1 in the (K_p, K_i)-plane; (e)–(g): Leading characteristic roots for cases A–C. (h): Critical stable frequency curve of Fig. 7(d).

which is similar to the non-CCC vehicle transfer function (14), except the different delay parameters. Reference [42] verified that string stability is unachievable for any selection of parameters when the driver response delay $\tau > t_h/2$ ($\approx 0.325s$), using the same non-CCC vehicle following model.

For simplicity and calculation, the following equivalent form of (18) is used:

$$P(\omega) = \left|\Gamma_{0,i}(j\omega)\right|^2 - 1 < 0, \quad \forall\omega > 0, \tag{24}$$

and substituting (22) into (24) leads to

$$\begin{aligned} P(\omega) &= [K_a^2\cos^2((\xi-\sigma)\omega) - \cos^2(\xi\omega) \\ &\quad + K_a^2\sin^2((\xi-\sigma)\omega) - \sin^2(\xi\omega)\,]\omega^6 \\ &\quad + [\,2K_p\sin(\xi\omega) + 2K_v\sin(\xi\omega) - 2K_aK_v\sin((\xi-\sigma)\omega)\,]\omega^5 \\ &\quad - [\,2K_pK_v + K_p^2 + 2f^*K_aK_p\cos((\xi-\sigma)\omega)\,]\omega^4 \\ &\quad + [\,2f^*K_aK_i\sin((\xi-\sigma)\omega) - 2f^*K_i\sin(\xi\omega) \\ &\quad - 2f^*K_p\sin(\xi\omega) - 2K_i\sin(\xi\omega)]\omega^3 + [2K_iK_p + 2K_iK_v \\ &\quad + 2f^*K_p^2 + f^{*2}K_p^2 + 2f^*K_iK_p + 2f^*K_pK_v]\omega^2 \\ &\quad - 2f^{*2}K_iK_p - f^{*2}K_p^2 - 2f^*K_i^2 - 2f^*K_iK_p - K_i^2 \end{aligned} \tag{25}$$

The meaning of (24) is that the satisfied ω needs to be positive and make $P(\omega) < 0$ for any selection of other parameters. If $P(\omega)$ reaches its maximum at $\omega_{cr} = 0$, from (25), then the stability condition (24) satisfied to $K_i > 0$ and $K_p > 0$.

According to (19), (22), and (24), Fig.7 (a) plots the string stability area of scene S_1, which is filled with dark grey and enclosed by the blue curve. The configuration of relevant parameters is $K_i = 0.5$, $K_a = 0.5$, $\xi = 0.2$s and $\sigma = 0.15$s. Points D-F, which cross the string stability area and are on the same vertical line as points A-C, are also marked. Points D and F are on the upper and lower edges of the boundary, respectively. The critical frequency ω_{cr} corresponding to the string stability boundary is plotted in Fig. 7(b). Bode plots of points A-F are depicted in Fig. 7(c). From the points C to A in Fig. 7(a) and Fig. 7(c), it can be seen that as K_p increases, the corresponding critical frequency (the X-axis value of the first intersection between $|\Gamma(j\omega)| = 1$ and corresponding curve) increases as well. Curve E shows a string stable scenario where $\left|\Gamma_{0,i}(j\omega)\right|^2 < 1$ for $\forall\omega > 0$. On the other hand, when crossing the boundary with $\omega_{cr} > 0$, curve D and curve F show the marginal string stability, implying string instability for low frequencies in point F.

Similarly, the plant stability boundary in parametric form for the fixed parameter K_v is:

$$\begin{aligned} K_p &= \Omega^2\left(\Omega\sin(\Omega\xi) + f^*\cos(\Omega\xi) - K_v\right)/(\Omega^2 + f^{*2}), \\ K_i &= \Omega^2\cos(\Omega\xi) - fK_p. \end{aligned} \tag{26}$$

The plant and string stability boundaries in the (K_p, K_i)-plane are plot in Fig. 7(d), with the fixed values, $K_v = 0.5$, $K_a = 0.5$, $\xi = 0.2$s, and $\sigma = 0.15$s. The critical frequencies Ω and ω_{cr} corresponding to the stability boundary are plotted in Fig. 7(h).

In the following, the effects of different parameters on the stability will be discussed. When every packet is delivered, DSRC communication has the average communication delay $\sigma = 0.15$s [43]. The plant stability boundary (red solid curve) and the string stability boundary (blue solid curve) in the (K_p, K_v)-plane for different values of K_a when $\xi = 0.25$s and $K_i = 0.2$ are depicted in Fig. 8. Parameter value $K_a = 0$ means that there is no acceleration feedback, which is similar to the human driver model, and thus, the sensing delay here is equivalent to the driver response time. The delays $\xi = 0.25$s or $\tau = 0.25$s are close to the upper limit of the critical delay of human driver model, and lead to a smaller string stability boundary area. As can be seen from the figure, the presence of acceleration feedback delay can increase the

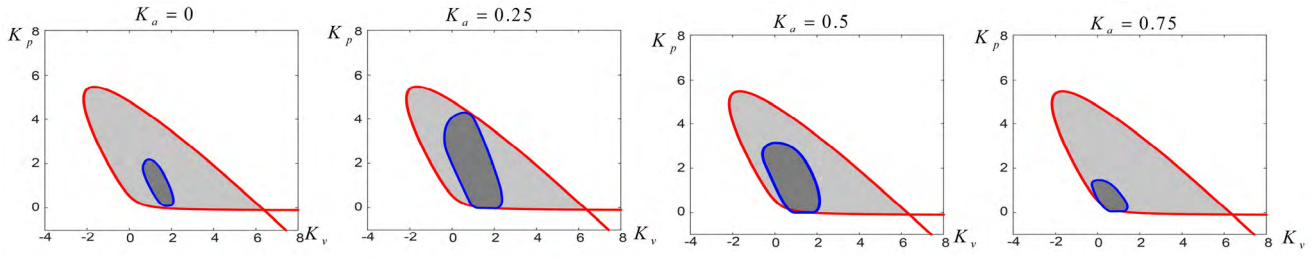

FIGURE 8. Stability diagram in the (K_p, K_v)-plane with different values of K_a. The same color notation is used as in Fig. 7(a).

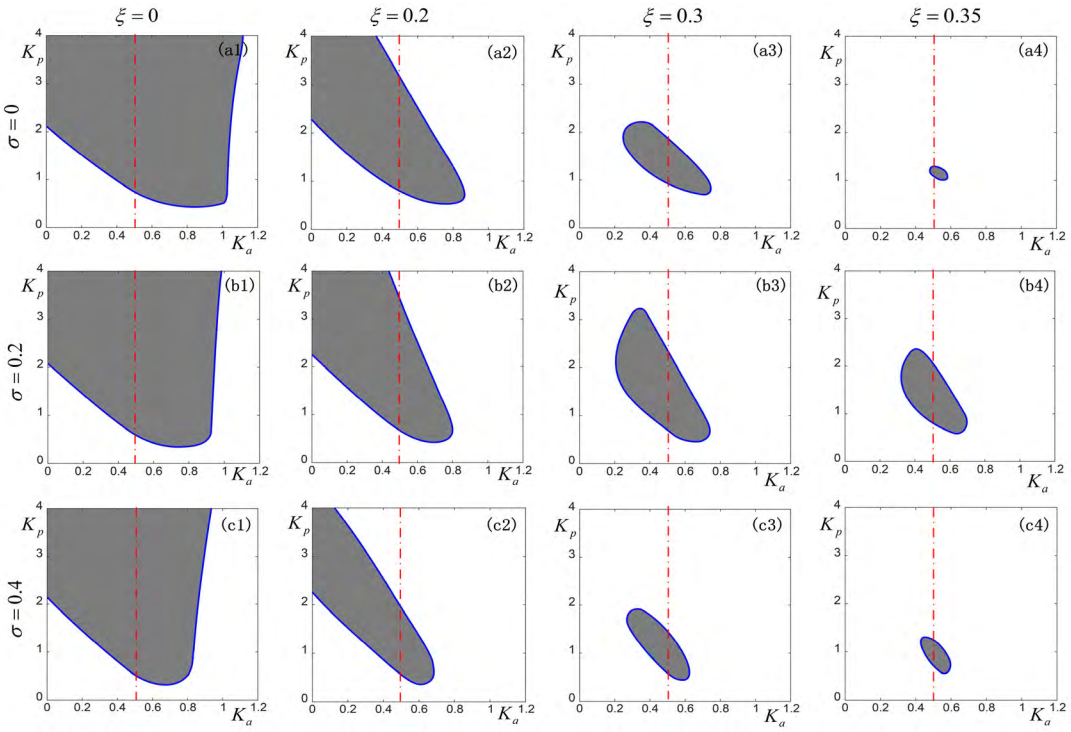

FIGURE 9. Head-to-tail string stable diagram in the (K_p, K_a)-plane.

string stability robustness, but excessive gain will reduce the stability area.

The stability charts in the (K_p, K_a)-plane for different delay values of ξ and σ, when K_i and K_v are both fixed as 0.5, are shown in Fig. 9. The string stability boundaries are plotted as blue curves enclosing the gray string stable area. Any gain parameters falling in the gray stable area can guarantee the string stability for any positive disturbance frequency.

As can be seen from Fig. 9(a1)-9(a4), the string stable area shrinks significantly when realistic sensing delay time ξ is greater than 0.35s, which means that no combination of parameters can satisfy the string stability, though the CCC vehicle can receive acceleration from the vehicle immediately ahead. It is obvious from Fig. 9 that the stability area becomes smaller under any communication delay when the sensing delay time increases, and the stability area boundary gradually shrinks towards the $K_a = 0.5$ line attachment.

The stability charts in the (K_p, K_a)-plane for different values of the communication delay σ, when $K_v = 0.5, \xi = 0.35$s and K_i equals to 0.2 or 0.5, are depicted in Fig. 10. It can be seen that after changing the value of K_i, the stable region still shrinks towards the red dotted line $K_a = 0.5$ attachment as the communication delay increases. Therefore, the string stability can be easier to maintain when choosing $K_a = 0.5$, which is more applicable.

The stability area increases first and then decreases when the communication delay σ increases from 0s to 0.4s, despite the value of K_i as 0.2 or 0.5. In this case, string stability boundary increases significantly when using appropriately designed communication delay, which means the critical sensing delay time ξ increases. This indicates a necessity of designing the communication delay σ when using acceleration feedback, instead of treating the communication delay σ as system limitations. Normally, the drive delay is fixed

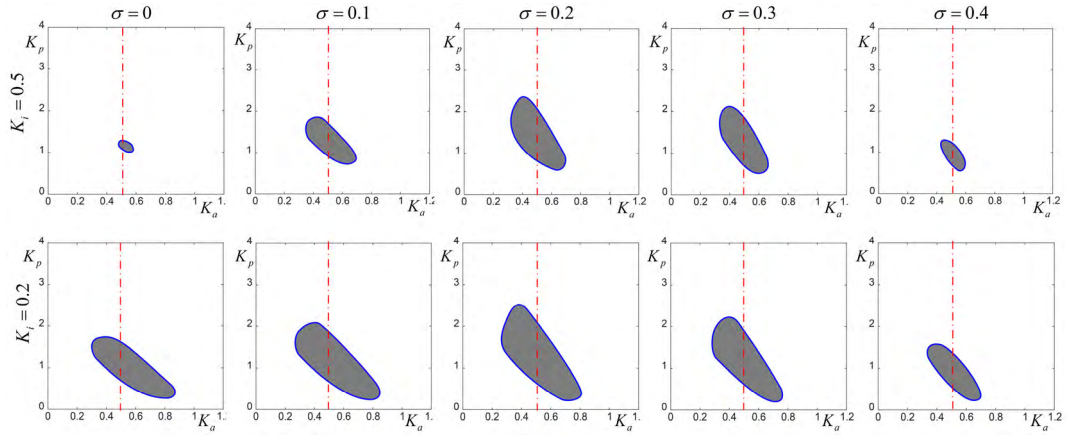

FIGURE 10. Head-to-tail string stable diagram in the (K_p, K_a)-plane for different values of K_i and σ.

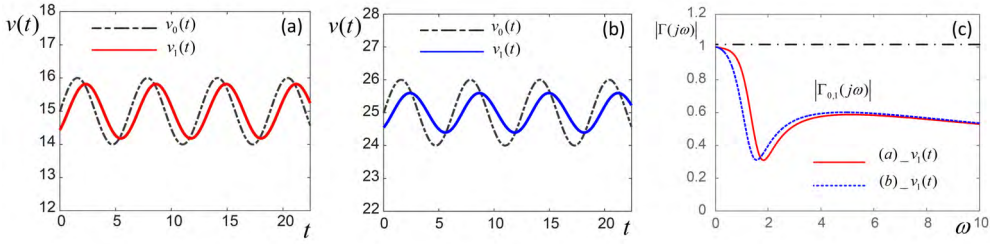

FIGURE 11. (a)-(b): Simulation results for S1 under different velocity, (c): Bode plot of CCC vehicle under different velocity.

and the value is small. The V2V communication delay may change with time. Thus, its effect on the stability of the host vehicle is also time-varying and difficult to quantify. From Fig 8 and Fig 9, it can be seen that the queue still achieves stability even when the controller has a certain communication delay and a small drive delay. Moreover, the corresponding stable area with $K_i = 0.2$ is larger than that with $K_i = 0.5$, demonstrating the stability area will shrink for higher value of K_i. In order to expand the stable range of the parameters, K_i is preferred to be set around 0.2.

For scene S_1, considering a head vehicle driven by a human driver, and perform simulations for the configuration with $K_p = 1$, $K_i = 0.2$, $K_v = 0.5$, $K_a = 0.5$, and $\sigma = 0.15$s, $\xi = 0.1$s. Fig. 11 depicts the different velocity responses of the CCC vehicle when the head vehicle (black dotted curve in Fig. 11(a) and 11(b), $v^* = 15$ m/s or $v^* = 25$m/s suffers from a periodic perturbation with frequency $\omega = 1$rad/s and amplitude $|\Delta v| = 1$ m/s. Red curve in Fig. 11(a) and blue curve in Fig. 11(b) show the following velocity of the CCC vehicle under low and high speed scenarios respectively. Fig. 11(c) depicts the bode plot under different velocities. The velocity response and bode plot of the CCC vehicles show that the CCC vehicle can attenuate disturbances.

To demonstrate superiority of the proposed range policy for CCC vehicle in (8), considering a situation where a side-vehicle merges into the clearance under the situation shown in Fig. 12(a). In the actual simulation process, T_s is set as $3L_{sy}/2v_{sy}$ and the maximum warning time is increase to 1.5s. Fig. 13 shows the factor η, velocity, acceleration and headway responses when the side-vehicle merges into the platoon suddenly. In the process of the side-vehicle approaching the target lane, the coefficient η stays to be zero until the lateral distance L_{sy} decrease to 0.5m, as shown in Fig. 13(a). In Fig. 13(b, c, d), red solid curve represents the responses of CCC vehicle under range policy (8), blue solid curve represents the responses of CCC vehicle under range policy (3), which recognizes the inserting side-vehicle as the following target vehicle only when the lateral distance between the sides of the side-vehicle and host vehicle (denoted as L_{sy} in Fig. 4) decreases to zeros.

Result shows that the CCC vehicle will brake down and change the headway from the lead vehicle in advance when the new rang policy is adopted. This caters more to the realistic situation as it is natural for the driver to brake at the sight of the side-vehicle's steering taillights. Benefited from the proposed strategy, the velocity fluctuation of the CCC vehicle is suppressed as red curve in Fig. 13(b). In addition, it is obvious from the red curve in Fig.13(c) that the braking is smoother compared with the blue curve using the traditional range policy of (3). In order to make the simulation of the vehicle driving process more realistic, In order to the simulation of the vehicle driving

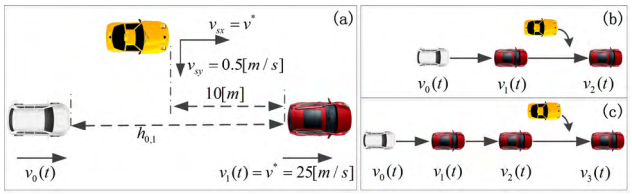

FIGURE 12. Merging behavior of the side-vehicle (yellow) in different platoon scenarios.

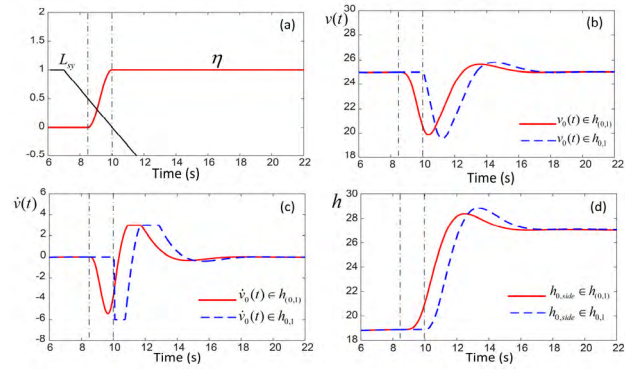

FIGURE 13. Responses of CCC vehicle when the side-vehicle merges into the platoon suddenly.

process more realistic, the vehicle acceleration range is limited between -6m/s^2 and 3m/s^2. Early braking can improve the safety of driving and smooth braking can improve the ride comfort. Fig. 13(d) shows that the CCC vehicle can reach a new equilibrium distance (red curve in Fig. 13(d)) faster than the traditional range policy (3). These simulation results demonstrate that the range policy considering the merging behavior of the side-vehicle can improve the string stability of vehicle platoon, and such improvements are beneficial for driving safety.

B. STABILITY DIAGRAMS FOR S_N

In this section, a conservative case where all vehicles (except the tail CCC vehicle) are driven by human drivers for scene S_2 and S_3 are considered. The head-to-tail transfer functions as follows:

$$\Gamma_{0,2}(s) = \frac{\tilde{V}_0(s)}{\tilde{V}_2(s)} = \frac{(F(s))^2 + E_1(s)F(s) + E_2(s)G(s)}{G(s)H(s)} \quad (27)$$

$$\Gamma_{0,3}(s) = \frac{\tilde{V}_0(s)}{\tilde{V}_2(s)} = \frac{F^3(s)+F^2(s)E_1(s)+F(s)E_2(s)G(s)+E_3(s)G^2(s)}{G^2(s)H(s)} \quad (28)$$

It can be seen that the plant stability is only related to $G^{n-1}(s)^*H(s)$, and the (16) of $G(s)$ and $H(s)$ are similar except for the delay parameters values ξ and τ. Fig. 14 shows the plant stability charts in the (K_p, K_v)-plane and (K_p, K_i)-plane for different time delay value, with $K_a = 0.5$ and $\sigma = 0.15$ s. The boundary curve corresponding to a

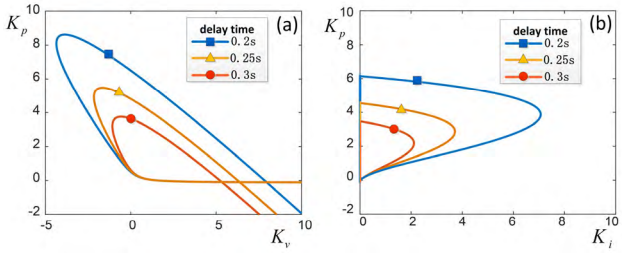

FIGURE 14. Plant stable diagram in the (K_p, K_v)-plane or (K_p, K_i)-plane. (a) $K_i = 0.2$; (b) $K_v = 0.5$.

smaller time delay can completely surround that corresponding to a larger one. Therefore, the plant stability boundary corresponding to the larger time delay can be regarded as the overall plant stability boundary.

For different values of communication delay σ and human reaction time τ, the stability diagrams for S_2 and S_3 in (K_p, K_v)-plane are shown in Fig. 15, with $K_a = 0.5$, $K_i = 0.2$, $\sigma = 0.15$ s and $\xi = 0.1$ s. Red solid curve indicates the plant stability boundary, and the string stability boundaries are depicted by the other color (blue, yellow, and dark yellow). The stability diagrams for S_2 and S_3 imply that the CCC vehicle can achieve the head-to-tail string stability in the platoon containing more than one vehicle ahead and the velocity disturbance of the head vehicle will not be amplified in the cruising process. As the human reaction time τ increases, the head-to-tail string stable domain sharply decreases. Therefore, it is better to have fewer human-driven vehicles in the communication chain. Since the head-to-tail string stability boundary is significantly influenced by the link length, the link length should be limited to maintain the string stability. In actual highway traffic flow, the distance between adjacent vehicles in the same lane can reach 30m (not including the vehicle length), when the vehicle speed exceeds 100km/h and range policy (3) is used. In addition, the effective V2V transmission distance is within 200m [44], thus the acceleration information of remote vehicles beyond the V2V transmission scope has little reference value. Therefore, we did not analyze the stability effects of more vehicles.

Similarly, simulations with merging behavior under the scene of S_2 and S_3 are conducted and shown in Fig. 12(b) and 12(c), with parameters $K_p = 1$, $K_v = 0.5$, $K_i = 0.2$, $K_a = 0.5$, $\sigma = 0.15$ s, and $\xi = 0.1$ s. Assuming that the side-vehicle have the same cut-in state as shown in Fig. 12(a). In the following, setting the human reaction time $\tau = 0.4$s, larger than the critical delay, which implies that human drivers typically cannot maintain string stability in the mid-headway range. Fig. 16(a) and 16(d) depict normal queue following state of S_2 and S_3, the head vehicle (black dotted curve) applies a periodic perturbation with frequency $\omega = 1$rad/s and amplitude $|\Delta v| = 1$ m/s. The green curve (tail car) represents the effect of CCC vehicles following the platoon vehicle. Fig. 16(b) and 16(e) depict the speed response of the vehicle in the platoon when the side-vehicle merging into the target lane, the red curve represents the velocity of

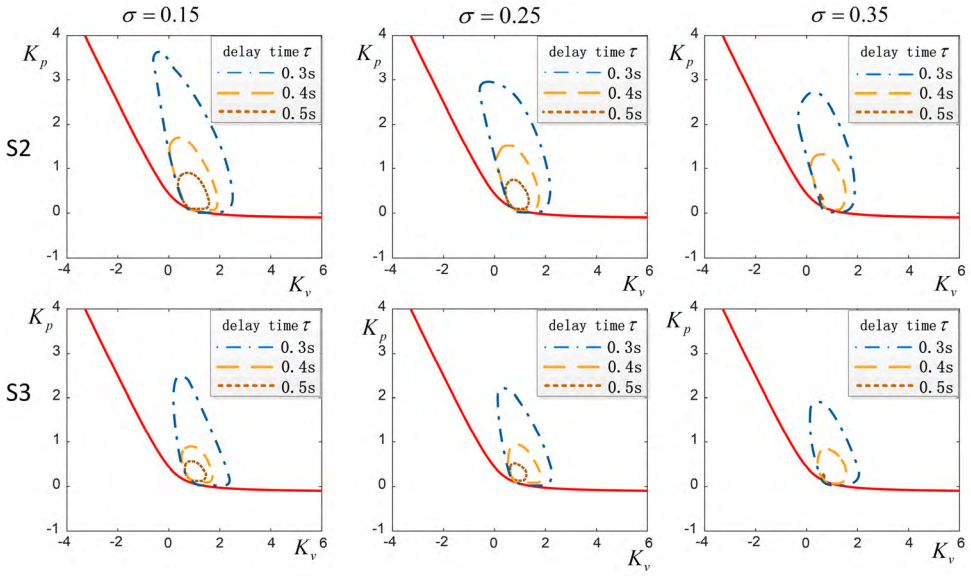

FIGURE 15. Stability diagram of S_2 and S_3 in (K_p, K_V)-plane with different human reaction time.

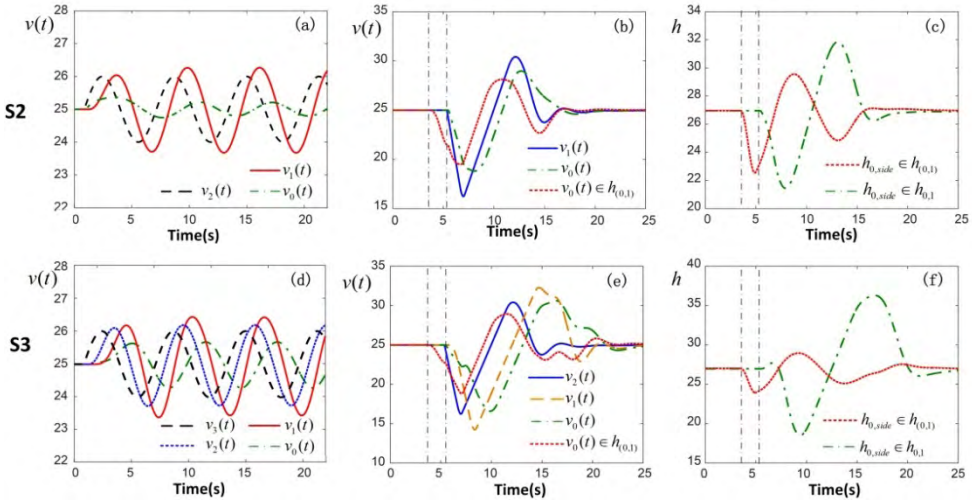

FIGURE 16. Simulation results of CCC vehicle response in S_2 and S_3.

CCC vehicles using range policy (8), the blue curve represents the velocity of CCC vehicles using range policy (3), and other colored lines represent additional vehicles inside the platoon. Fig. 16(c) and 16(f) depict the distance between CCC vehicles and the side-vehicle of two scenarios.

Fig. 16(a) and 16(d) show that the CCC vehicle (green curve) can attenuate the disturbance (red and blue curve) caused by the human driver's reaction delay. Fig 16(b) and 16(e) show that the CCC vehicle (red curve) can be braked down and change the headway from the lead vehicle in advance, and achieve the final stable balance with smaller speed fluctuations by adapting range policy with side-vehicle merging behavior. At the same time, it can be seen from Fig. 16(e) and 16(d) that more human drivers will lead to greater speed fluctuations of backward transmission and longer fluctuation time. Fig. 16(c) and 16(f) show that under the two range policy, CCC vehicle can both reach the equilibrium state.

C. EXPERIMENT PLATFORM AND RESULTS

As shown in Fig. 17, the experimental platforms are built based on two electric vehicles. Due to the limited number of test vehicles and equipment, we just set up a queue test for two cars, and the experiments and tests are carried out in low-speed situation within the campus environment. The Cohda Wireless MK5 OBU module is adopted in both cars for vehicle-to-vehicle communication, and the fusion forward vision system is installed on the host vehicle for target snap. Both vehicles are equipped with the NAV-982 inertial navigation system. The host vehicle realizes CAN bus control

FIGURE 17. Experimental platform and test scenario.

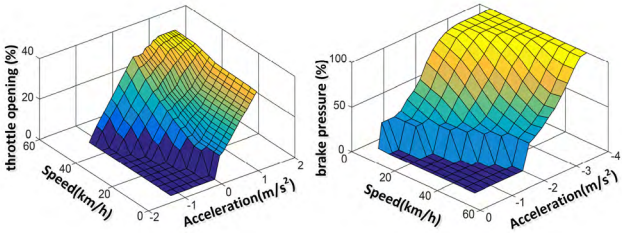

FIGURE 18. Acceleration and braking control information.

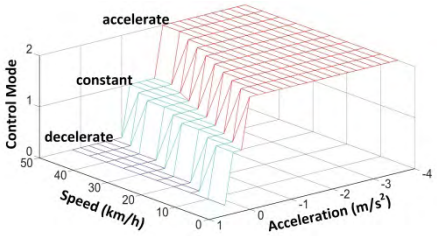

FIGURE 19. Acceleration mode switching diagram.

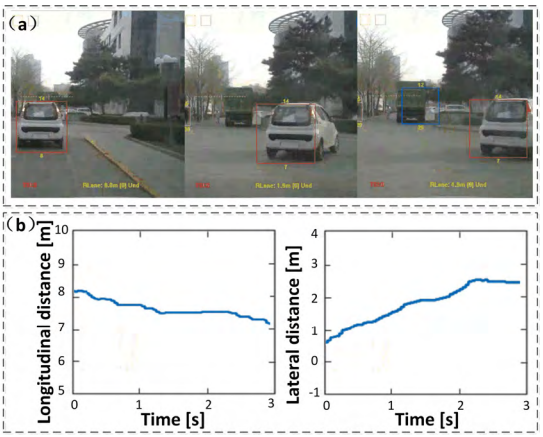

FIGURE 20. Results of lateral movement of target vehicle.

through electronic control modification. To simplify the nonlinear effects of the motor, retarder, tire and wind resistance, the vehicle dynamic response characteristics are simplified to the inverse dynamic model. Fig. 18 shows the relationship of throttle and brake pressure mapping to different speed and acceleration pairs, thus the control signals can be obtained by searching the map with expected acceleration of (9).

To avoid frequently accelerating and decelerating switching when driving at a constant speed, we tested the taxi acceleration at different vehicle speeds and appropriately relaxed the acceleration control interval when the vehicle was at a constant speed, as shown in Fig. 19.

Due to the limited number of test vehicles and equipment, a queue with two cars is established. Besides, in order to accurately control the motion state of the side-vehicle, kinematic model is employed to simulate the real side-vehicle merging behavior, which makes it capable for simultaneously triggering and can facilitate the comparison test by setting the same side behavior state.

Since the target captured by the visual system is the original scatter target, we determine the effectiveness of the vehicle target in the road based on the slide-window detector. Fig. 20(a) shows the right-turning target vehicle (red box) monitored by the visual system. Fig. 20(b) shows the relative longitudinal velocity and distance of the target after filtering. As can be seen from the figure, the calculated distance data is less noisy, and the relative lateral distance gradually increases with the right transition of the target vehicle. The target vehicle gradually disappears into the field of view at a distance of 7m in the longitudinal direction and 2.5m in the lateral direction of the axle. The monitoring strategy in this paper only considers the lateral distance within 1m of the vehicle's edge. It can be considered that the vision system can accurately obtain the target information.

Based on the design and analysis of the controller mentioned above, this paper carries out the following real vehicle experiments: (1) the host vehicle follows the preceding vehicle without using acceleration information, (2) using acceleration signal, and (3) using acceleration information together with side-vehicle merging behavior. The preceding vehicle is driven by an experienced driver, while the host vehicle is controlled by our designed controller. The time synchronization between two vehicles is realized by adding delay in the controller. The sensor delay of our vehicle is a constant value, and the V2V equipment has a universal average delay value of 0.15s. The controller parameters are consistent with the simulation parameters of Fig. 11, with $K_p = 1$, $K_i = 0.2$, $K_v = 0.5$, $K_a = 0.5$, $\sigma = 0.15$ s, and $\xi = 0.1$ s. The corresponding speed response curves are drawn in Fig. 21(a), 21(b), and 21(c).

Fig. 21(a) shows the speed fluctuation of the host vehicle. Fluctuation is amplified when the host vehicle follows the leading vehicle. Fig. 21(b) shows the speed curve of the host vehicle and the preceding vehicle considering acceleration information. We can see that the host vehicle can quickly respond to the speed change of the preceding vehicle and maintain the speed consistency of the host vehicle speed. The speed fluctuation transmitted to the host vehicle is not amplified, which can ensure the stability of the queue. From the two pictures, it can be observed that the speed change response will lag behind the previous car because of the communication delay and the driving delay. Using acceleration information can improve the stability of the queue. No matter

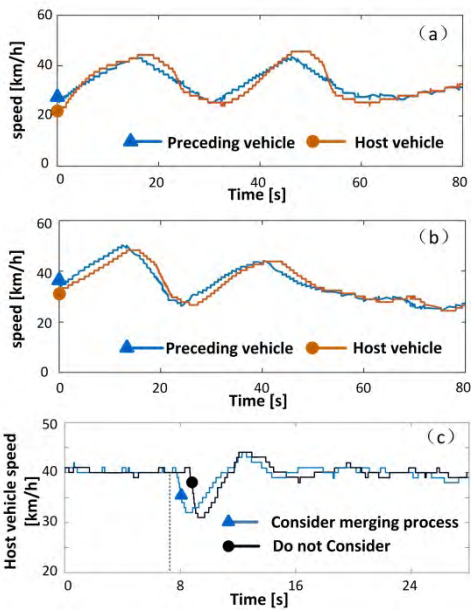

FIGURE 21. Experimental results under different following scenario.

whether acceleration information is used or not, the controller can ensure the plant stability of the vehicle, and the host vehicle can reach the balance speed of the preceding vehicle. Using acceleration information can improve the stability of the queue.

By comparing the theoretical simulation with the real vehicle test, it is found that the following effect of the real vehicle is the same as the predicted trend, but with a larger control error. Because the driving delay and communication delay are both constant values in the theoretical analysis, while in the case of real vehicle control, the driving delay is a first-order inertia delay link and the communication delay varies in a small range. The added acceleration mode judgment is also one of the reasons that can affect the following error.

Fig. 21(c) shows the speed curve of the host vehicle when the side-vehicle appears. The dotted line indicates the starting point of the system when consider the lateral behavior of the side-vehicle. Result shows that the host vehicle can follow the preceding vehicle's driving speed well in these two test cases, and considering the side-vehicle merging process ensures that the host vehicle decelerates in advance, and the speed change is smaller. Test results are in good agreement with the simulation results. It proves that the CCC strategy mentioned in this paper can achieve earlier, faster and more accurate response in the case of side-vehicle merging process, ensuring the stability and security of the vehicle queue.

IV. CONCLUSION

In this paper, a new policy considering the side-vehicle merging behavior that is frequently happening at high speed driving queue is proposed. By designing and applying the new nonlinear range policy, the driving safety and riding comfort can be significantly improved when the side-vehicle merging behavior suddenly occurs.

The controller and follow-up strategy designed in this paper can ensure the existence of uniform flow equilibrium in the entire velocity range, in particular at the linear level. Transfer functions is used to evaluate the dynamics and convert the algebraic stability conditions into stability charts that allow designers to choose the control gains, make sure that the controller can attenuate with any preceding vehicle speed fluctuations that occur. Using the acceleration information of the preceding vehicle can significantly improve the stability of the queue. In addition, we also demonstrated that the gain of the acceleration feedback shall be preferred around 0.5, which is more widely used. In these surrounded domains the system showed string stable behavior for the ahead velocity perturbations, that is, perturbations decayed as they propagated backward along the chain of vehicles. The existence of proper communication delay is conducive to the improvement of stability, and human reaction time or sensing delay will reduce the string stability region. We also proved that increasing the number of CCC vehicles may provide a more stable follow effect, and can attenuating the speed fluctuations generated by human drivers more faster.

In the future, the optimization of acceleration gains for different link lengths and heterogeneity raised by non-identical human reaction time would be our next work, and set different communication delays for more real-world comparison experiments. Furthermore, it is also necessary to consider the influence of the sensor error of other vehicles on the stability of the host vehicle.

REFERENCES

[1] D. Caveney, "Cooperative vehicular safety applications," *IEEE Control Syst.*, vol. 30, no. 4, pp. 38–53, Aug. 2010.
[2] X. Xiang, W. Qin, and B. Xiang, "Research on a DSRC-based rear-end collision warning model," *IEEE Trans. Intell. Transp. Syst.*, vol. 15, no. 3, pp. 1054–1065, Jun. 2014.
[3] S. I. Guler, M. Menendez, and L. Meier, "Using connected vehicle technology to improve the efficiency of intersections," *Transp. Res. C, Emerg. Technol.*, vol. 46, pp. 121–131, Sep. 2014.
[4] R. H. Patel, J. Härri, and C. Bonnet, "A collision mitigation strategy for intelligent vehicles to compensate for human factors affecting manually driven vehicles," in *Proc. ITSC*, Oct. 2018, pp. 114–119.
[5] C. Suthaputchakun, Z. Sun, and M. Dianati, "Applications of vehicular communications for reducing fuel consumption and CO_2emission: The state of the art and research challenges," *IEEE Commun. Mag.*, vol. 50, no. 12, pp. 108–115, Dec. 2012.
[6] B. van Arem, C. J. G. van Driel, and R. Visser, "The impact of cooperative adaptive cruise control on traffic-flow characteristics," *IEEE Trans. Intell. Transp. Syst.*, vol. 7, no. 4, pp. 429–436, Dec. 2006.
[7] K. Yi and I.-K. Moon, "A driver-adaptive stop-and-go Cruise control strategy," in *Proc. IEEE Int. Conf. Netw., Sens. Control*, vol. 1, Mar. 2004, pp. 601–606.
[8] A. Kesting, M. Treiber, M. Schönhof, and D. Helbing, "Adaptive cruise control design for active congestion avoidance," *Transp. Res. C, Emerg. Technol.*, vol. 16, no. 6, pp. 668–683, 2008.
[9] J. Zhou and H. Peng, "Range policy of adaptive cruise control vehicles for improved flow stability and string stability," *IEEE Trans. Intell. Transp. Syst.*, vol. 6, no. 2, pp. 229–237, Jun. 2005.
[10] S. E. Shladover *et al.*, "Automated vehicle control developments in the PATH program," *IEEE Trans. Veh. Technol.*, vol. 40, no. 1, pp. 114–130, Feb. 1991.

[11] H. Fritz, "Longitudinal and lateral control of heavy duty trucks for automated vehicle following in mixed traffic: Experimental results from the CHAUFFEUR project," in *Proc. IEEE Int. Conf. Control Appl.*, vol. 2, Aug. 1999, pp. 1348–1352.

[12] T. Robinson, E. Chan, and E. Coelingh, "Operating platoons on public motorways: An introduction to the SARTRE platooning programme," in *Proc. ITS*, Busan, Korea, vol. 1, Oct. 2010, p. 12.

[13] S. Tsugawa and S. Kato, "Energy ITS: Another application of vehicular communications," *IEEE Commun. Mag.*, vol. 48, no. 11, pp. 120–126, Nov. 2010.

[14] R. Kianfar *et al.*, "Design and experimental validation of a cooperative driving system in the grand cooperative driving challenge," *IEEE Trans. Intell. Transp. Syst.*, vol. 13, no. 3, pp. 994–1007, Sep. 2012.

[15] S. Kokogias *et al.*, "Development of platform-independent system for cooperative automated driving evaluated in GCDC 2016," *IEEE Trans. Intell. Transp. Syst.*, vol. 19, no. 4, pp. 1277–1289, Apr. 2018.

[16] L. Zhang and G. Orosz, "Designing network motifs in connected vehicle systems: Delay effects and stability," in *Proc. ASME Dyn. Syst. Control Conf.*, 2013, p. V003T42A006.

[17] J. I. Ge and G. Orosz, "Dynamics of connected vehicle systems with delayed acceleration feedback," *Transp. Res. C, Emerg. Technol.*, vol. 46, pp. 46–64, Sep. 2014.

[18] W. B. Qin, M. M. Gomez, and G. Orosz, "Stability and frequency response under stochastic communication delays with applications to connected cruise control design," *IEEE Trans. Intell. Transp. Syst.*, vol. 18, no. 2, pp. 388–403, Feb. 2017.

[19] D. Swaroop, J. K. Hedrick, C. C. Chien, and P. Ioannou, "A comparision of spacing and headway control laws for automatically controlled vehicles," *Vehicle Syst. Dyn.*, vol. 23, no. 1, pp. 597–625, 1994.

[20] Y. Zheng, S. E. Li, J. Wang, L. Y. Wang, and K. Li, "Influence of information flow topology on closed-loop stability of vehicle platoon with rigid formation," in *Proc. IEEE Int. Conf. Intell. Transp. Syst.*, Oct. 2014, pp. 2094–2100.

[21] S. E. Li, Y. Zheng, K. Li, and J. Wang, "Scalability limitation of homogeneous vehicular platoon under undirected information flow topology and constant spacing policy," in *Proc. 34th Chin. Control Conf.*, Jul. 2015, pp. 8039–8045.

[22] L. Zhang and G. Orosz, "Motif-based design for connected vehicle systems in presence of heterogeneous connectivity structures and time delays," *IEEE Trans. Intell. Transp. Syst.*, vol. 17, no. 6, pp. 1638–1651, Jun. 2016.

[23] P. Wang, Z. Sun, J. Tan, Z. Huang, Q. Zhu, and W. Zhao, "Development and evaluation of cooperative adaptive cruise controllers," in *Proc. IEEE Int. Conf. Mechatron. Automat.*, Aug. 2015, pp. 1607–1612.

[24] H. Kazemi, H. N. Mahjoub, A. Tahmasbi-Sarvestani, and Y. P. Fallah, "A learning-based stochastic MPC design for cooperative adaptive cruise control to handle interfering vehicles," *IEEE Trans. Intell. Vehicles*, vol. 3, no. 3, pp. 266–275, Sep. 2018.

[25] F. E. Sancar, B. Fidan, J. P. Huissoon, and S. L. Waslander, "MPC based collaborative adaptive cruise control with rear end collision avoidance," in *Proc. Intell. Vehicles Symp. Proc.*, Jun. 2014, pp. 516–521.

[26] Y. Zhu and D. Zhao, "Comprehensive comparison of online ADP algorithms for continuous-time optimal control," *Artif. Intell. Rev.*, vol. 49, no. 4, pp. 531–547, 2017.

[27] D. Zhao, Z. Hu, Z. Xia, C. Alippi, Y. Zhu, and D. Wang, "Full-range adaptive cruise control based on supervised adaptive dynamic programming," *Neurocomputing*, vol. 125, pp. 57–67, Feb. 2014.

[28] F. Guo, B. M. Wotring, and J. F. Antin, "Evaluation of lane change collision avoidance systems using the national advanced driving simulator," Nat. Highway Traffic Saf. Admin., Washington, DC, USA, Tech. Rep. DOT HS 811-332, May 2010.

[29] H. M. Mandalia and M. D. D. Salvucci, "Using support vector machines for lane-change detection," in *Proc. Hum. Factors Ergonom. Soc. Annu. Meeting*, vol. 49, no. 22, pp. 1965–1969, 2005.

[30] R. S. Tomar, S. Verma, and G. S. Tomar, "Prediction of lane change trajectories through neural network," in *Proc. Int. Conf. Comput. Intell. Commun. Netw.*, Nov. 2010, pp. 249–253.

[31] A. Wahab, C. Quek, C. K. Tan, and K. Takeda, "Driving profile modeling and recognition based on soft computing approach," *IEEE Trans. Neural Netw.*, vol. 20, no. 4, pp. 563–582, Apr. 2009.

[32] H. Berndt, J. Emmert, and K. Dietmayer, "Continuous driver intention recognition with hidden Markov models," in *Proc. IEEE 11th Int. Conf. Intell. Transp. Syst.*, Oct. 2008, pp. 1189–1194.

[33] M. Mori, C. Miyajima, T. Hirayama, N. Kitaoka, and K. Takeda, "Integrated modeling of driver gaze and vehicle operation behavior to estimate risk level during lane changes," in *Proc. IEEE 16th Int. Conf. Intell. Transp. Syst.*, Oct. 2013, pp. 2020–2025.

[34] Q. Wang, Z. Li, and L. Li, "Investigation of discretionary lane-change characteristics using next-generation simulation data sets," *J. Intell. Transp. Syst.*, vol. 18, no. 3, pp. 246–253, 2014.

[35] L. Zhang and G. Orosz, "Beyond-line-of-sight identification by using vehicle-to-vehicle communication," in *Proc. IEEE Trans. Intell. Transp. Syst.*, vol. 19, no. 6, pp. 1962–1972, Jun. 2018.

[36] G. Orosz, R. E. Wilson, and G. Stépán, "Traffic jams: Dynamics and control," *Philos. Trans. Roy. Soc. A*, vol. 368, no. 1928, pp. 4455–4479, 2010.

[37] W. B. Qin, M. M. Gomez, and G. Orosz, "Stability analysis of connected cruise control with stochastic delays," in *Proc. Amer. Control Conf.*, Jun. 2014, pp. 4624–4629.

[38] F. Bai and H. Krishnan, "Reliability analysis of DSRC wireless communication for vehicle safety applications," in *Proc. IEEE Intell. Transp. Syst. Conf.*, Sep. 2006, pp. 355–362.

[39] P. Seiler, A. Pant, and K. Hedrick, "Disturbance propagation in vehicle strings," *IEEE Trans. Autom. Control*, vol. 49, no. 10, pp. 1835–1842, Oct. 2004.

[40] K. Engelborghs, T. Luzyanina, and G. Samaey, "DDE-BIFTOOL: A MATLAB package for bifurcation analysis of delay differential equations," Dept. Comput. Sci., KU Leuven, Leuven, Belgium, TW, Rep. 305, Mar. 2000.

[41] G. Stépán, "Retarded dynamical systems: Stability and characteristic functions," Pitman Res. Notes Math, Longman Sci. & Tech., Harlow, U.K., Tech. Rep. 210, 1989.

[42] G. Orosz, "Connected cruise control: Modelling, delay effects, and nonlinear behaviour," *Vehicle Syst. Dyn.*, vol. 54, no. 8, pp. 1147–1176, 2016.

[43] W. B. Qin and G. Orosz, "Digital effects and delays in connected vehicles: Linear stability and simulations," in *Proc. ASME Dyn. Syst. Control Conf.*, 2013, p. V002T30A001.

[44] Y. Gunter and H. P. Grobmann, "Usage of wireless LAN for inter-vehicle communication," in *Proc. IEEE Intell. Transp. Syst.*, Sep. 2005, pp. 408–413.

TAO ZHANG received the M.S. degree from the Beijing University of Technology, China, in 2015. He is currently pursuing the Ph.D. degree with the Beijing Institute of Technology, China. His current research interests include the hardware design of vehicle controller, vehicle dynamics control, advanced driver assistance systems, and reinforcement learning.

YUAN ZOU received the Ph.D. degree from the Beijing Institute of Technology, in 2005. He is currently a Professor with the Beijing Collaborative and Innovative Center for Electric Vehicles and the School of Mechanical Engineering, Beijing Institute of Technology. He is also the Co-Director of the ETHZ-BIT Joint Research Center for New Energy Vehicle Dynamic System and Control. He conducted research in the field of ground vehicle propulsion modeling and optimal control at the University of Michigan, Ann Arbor, and ETH Zurich. His research interests include modeling and control for electrified vehicle and transportation systems.

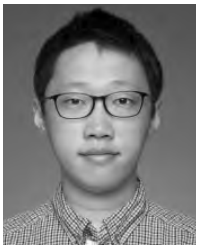

XUDONG ZHANG received the M.S. degree in mechanical engineering from the Beijing Institute of Technology, Beijing, China, in 2011, and the Ph.D. degree in mechanical engineering from the Technical University of Berlin, Berlin, Germany, in 2017. Since 2017, he has been an Associate Professor with the Beijing Institute of Technology. His main research interests include distributed drive electric vehicles, vehicle dynamics control, vehicle state estimation, and torque allocation.

NINGYUAN GUO received the B.S. degree in mechanical design and automation from the Shanghai University of Engineering Sciences, Shanghai, China, in 2014, and the M.S. degree in automobile engineering from the Kunming University of Science and Technology, Kunming, China, in 2018. He is currently pursuing the Ph.D. degree in automobile engineering with the Beijing Institute of Technology, Beijing, China. His research interests include vehicle dynamics control, distributed drive electric vehicles, and power management of hybrid electric vehicles. He was a recipient of the National Scholarship, China, in 2017, and the Second Place of the IEEE VTS Motor Vehicles Challenge, in 2017 and 2018.

WENWEI WANG received the Ph.D. degree from the School of Mechanical and Vehicular Engineering, Beijing Institute of Technology, China, in 2007. He is currently an Associate Professor with the Mechanical and Vehicular Engineering School, the Assistant Dean of the New Energy Automotive Research Institute, and the Deputy Director of the Beijing Electric Vehicle Collaborative Innovation Center, Beijing Institute of Technology. His current research interests include structure mechanics of vehicle body, battery mechanics, vehicle dynamics, and electromechanical coupling dynamics.